Control of Airy-beam self-acceleration by photonic lattices

Falko Diebel,[1,*] Bojana M. Bokić,[2] Martin Boguslawski,[1] Aleksandra Piper,[2] Dejan V. Timotijević,[2] Dragana M. Jović,[2] and Cornelia Denz[1]

[1]*Institut für Angewandte Physik and Center for Nonlinear Science (CeNoS), Westfälische Wilhelms-Universität Münster, 48149 Münster, Germany*

[2]*Institute of Physics, University of Belgrade, P.O. Box 68, 11001 Belgrade, Serbia*

(Received 3 June 2014; published 2 September 2014)

We demonstrate control over the acceleration of two-dimensional Airy beams propagating in optically induced photonic lattices. Depending on the lattice strength, we observe a slowing-down and suppression of the self-acceleration of Airy beams, as well as a formation of discrete lattice beams. Moreover, we explore the effects of different artificial single-side defects on the propagation and acceleration. For positive defects, the localization of the Airy beam to the defect site is further enhanced, while for negative defects most of the power is repelled from this site.

DOI: 10.1103/PhysRevA.90.033802 PACS number(s): 42.40.Jv, 42.25.Fx, 42.70.Nq

I. INTRODUCTION

Since their discovery in 1979 by Berry and Balazs [1], the fascinating class of Airy beams has attracted huge interest in different fields of physics. Originally, Airy beams were introduced as wave functions, solving the one-dimensional Schrödinger equation for free particles. Their probability density remarkably stays nonspreading under time evolution, while being transversely accelerated to follow a parabolic trajectory. Due to the formal equivalence between the Schrödinger equation in quantum mechanics and the paraxial equation of diffraction in optics, the concepts and solutions can be transferred to optics, where Airy beams can be directly observed and explored in experiments.

The first realization of optical one- and two-dimensional Airy beams [2] initiated an active field of research, leading to a number of systematic investigations of the generation, the manipulation, and the general properties of Airy beams in linear and nonlinear regimes [3–8]. The unique nonspreading and self-accelerating features of Airy beams moreover led to a huge variety of applications, including so-called autofocusing beams [9], optical snowblowers [10], and optical routers [11]. Also the influence of inhomogeneous potentials and the presence of dielectric interfaces on the propagation of Airy beams have been studied in the past [8,12–17].

Controlling the propagation behavior of light with light itself is the key requirement to realize new all-optical guiding and switching architectures. It is well known that the presence of discrete photonic lattice structures dramatically changes the propagation dynamics of light. Thus, one promising approach towards this goal is to tailor the transverse acceleration of two-dimensional optical Airy beams using photonic lattices. Recently, defect guided Airy beams in optically induced one-dimensional waveguide arrays were observed [18]. Despite the fact that Airy beams have been subject to many research activities, the propagation of such accelerated beams inside a two-dimensional optically induced photonic lattice has only been studied numerically with an isotropic refractive index potential assumed [19].

In this paper, we investigate and analyze the propagation dynamics of self-accelerating Airy beams in two-dimensional photonic lattices including defects, both theoretically and experimentally. The lattices were fabricated by optical induction [20] in photorefractive strontium barium niobate and the refractive index modulations are numerically calculated in the anisotropic model [21]. We consider how the discrete lattice changes the shape of the Airy beam and influences its self-acceleration. The propagation dynamics and beam acceleration are controlled by varying the lattice strength. We find that increasing the refractive index modulation reduces the Airy beam acceleration and leads to the formation of discrete lattice beams. Additionally, we realize different defect lattices by embedding two types of single-site defects into the regular lattice and investigate the impact onto the Airy beam. The defects remarkably change the beam dynamics. For the negative defect the beams experience a strong repulsion, while in the presence of the positive defect they form strongly localized waves or defect modes.

II. THEORETICAL BACKGROUND AND EXPERIMENTAL SETUP

To study the propagation characteristics of Airy beams in an optical system with induced photonic lattices, we consider the scaled paraxial equation of diffraction for the electric field Ψ:

$$i\frac{\partial\Psi}{\partial\zeta}+\frac{1}{2}\left(\frac{\partial^2\Psi}{\partial\chi^2}+\frac{\partial^2\Psi}{\partial\nu^2}\right)+\frac{1}{2}k_0^2w_0^2\Delta n^2(I_{\mathrm{indu}})\Psi=0. \quad (1)$$

Here, $\chi=x/\mathrm{w}_0$ and $\nu=y/\mathrm{w}_0$ are the dimensionless transverse coordinates scaled by the characteristic length w_0. $\zeta=z/k\mathrm{w}_0^2$ represents the dimensionless propagation distance with $k=2\pi n/\lambda$. The photonic lattice enters this equation in terms of an intensity-dependent refractive index modulation $\Delta n^2(I_{\mathrm{indu}})$, which is described by the full anisotropic model [21] and precisely models the optical induction process in an externally biased photorefractive crystal. Moreover, Eq. (1) is also suitable to cover nonlinear light propagation when the inducing intensity becomes a function of the field Ψ itself. In this contribution, however, we restrict ourselves to linear effects.

*Corresponding author: falko.diebel@uni-muenster.de

For the case of linear light propagation in homogenous media, where $\Delta n^2 = 0$, the wave equation (1) can always be separated into two parts, each depending only on one transverse coordinate, χ or ν, respectively. Consequently, also the solution Ψ separates and can be written as product in the following form: $\Psi(\chi,\nu,\zeta) = \psi(\chi,\zeta)\psi(\nu,\zeta)$, where ζ is the longitudinal coordinate. As first shown in Ref. [1], each part of the wave equation can be solved by a nondispersive one-dimensional Airy function $\mathrm{Ai}(X)$. Thus, the overall solution of Eq. (1) in two dimensions reads as

$$\Psi(\chi,\nu,\zeta) = \psi(\chi,\zeta)\psi(\nu,\zeta) \tag{2}$$

with

$$\psi(X,\zeta) = \mathrm{Ai}[X - (\zeta/2)^2]\exp[i(X\zeta/2) - i(\zeta^3/12)] \tag{3}$$

and $X = \{\chi,\nu\}$.

The solution $\Psi(\chi,\nu,\zeta)$ describes a nonspreading, two-dimensional optical Airy beam which is transversely accelerated while propagating along the longitudinal coordinate ζ. At first glance, the acceleration of the wave packets in homogeneous media without any index gradient seems to contradict the Ehrenfest theorem, which states that the center of mass of a wave function moves with constant speed if there is no force acting. Since Ψ is not square integrable, the center of mass cannot be defined. This also implies that the wave function contains infinite energy and extends over the whole space, both being nonphysical [6,22].

We instead have to consider a truncated solution with finite extent and energy, written as $\psi(X,0) = \mathrm{Ai}[X]\exp[a_X X]$, with the positive decay length a_X, typically $a_X \ll 1$. It has been shown that this truncated solution still solves the wave equation (1) and that the distinguished properties of two-dimensional Airy beams are mostly preserved [23]. Although the truncated intensity pattern is now nonspreading only over a limited propagation distance, this easily covers the longitudinal range which is necessary to observe sufficient transverse displacement of the Airy beam.

The characteristics of a two-dimensional optical Airy beam propagating inside a homogeneous medium are shown experimentally in Fig. 1. The transverse intensity distributions of the Airy beam at the front and the back faces of the photorefractive crystal are shown in Figs. 1(b) and 1(c), respectively. In addition, the intensity profile is recorded for a huge set of transverse planes along the crystal to demonstrate the accelerated transverse shift of the Airy beam during propagation. A cross section through this three-dimensional intensity volume along one vertical axis is shown in Fig. 1(a). This picture reveals that the experimentally realized Airy beam follows the expected accelerated trajectory and it proves that the unavoidable truncation with $a_{\chi,\nu} \neq 0$ in the experiment only negligibly affects the beam propagation compared to the ideal case of infinite beams.

A. Optically induced photonic lattices

To experimentally realize the photonic lattices for controlling the acceleration of the Airy beam we use the technique of optical induction [20], which in the past has proved its flexibility to create various types of two- and three-dimensional photonic lattices [24–26]. Moreover, this approach provides a versatile platform to study different fundamental linear and nonlinear propagation effects, such as Anderson localization [27] or discrete lattice and vortex solitons [28,29].

The optical induction method relies on the property of photorefractive materials, e.g., strontium barium niobate (SBN), to locally change their refractive index according to the intensity distribution the crystal is illuminated with [30]. For this reason the resulting refractive index structure is directly linked to the intensity of the induction beam. In all experiments presented in this contribution we require two-dimensional photonic lattices, implying that the induction beam may be conveniently realized by choosing from the wide class of nondiffracting beams [31,32].

For the realization of photonic lattices with the optical induction technique, we use nondiffracting beams characterized by optical fields whose intensity distributions are modulated in the transverse plane and stay unchanged in the longitudinal dimension. Such beams share the property that in Fourier space all contributing field components lie on an infinitely small ring with radius k_t, defining the structure size of the transverse pattern in real space. In particular, we consider a photonic square lattice which would be constituted from superimposing four tilted plane waves. The electric field E_{ndB} then reads as

$$E_{\mathrm{ndB}}(x,y,z) = \sum_{n=1}^{4} E_n e^{ik_t(x\cos\varphi_n + y\sin\varphi_n)} e^{ik_z z}, \tag{4}$$

with $\varphi_n = \pi(2n+1)/4$ and $k^2 = k_t^2 + k_z^2$. To minimize the anisotropic response of the photorefractive effect, the induction beam is rotated by 45°.

Figure 1(d) shows the recorded intensity distribution of the experimentally realized nondiffracting beam which is used to optically induce the two-dimensional square lattice. The lattice period $\Lambda = \pi/k_t \approx 25\mu\mathrm{m}$ is chosen to exactly match the distance between the main and the next neighboring lobes of the Airy beam. To realize different lattice strengths Δn, we utilize that the optically induced refractive index modulation in SBN builds up with time. By illuminating the crystal with the writing beam intensity for different times we thus are able to control the depths of the index modulation. To verify that the appropriate photonic lattice is actually induced, we illuminate the front face of the crystal with a plane wave after the writing process was completed. The initially homogeneous intensity of the plane wave is redistributed by the imprinted refractive index modulation to be locally increased at regions of higher refractive index. Thus, by recording the intensity at the back face of the crystal we can visualize the written photonic structure [Fig. 1(e)] [24].

B. Experimental setup and numerical methods

All experiments were carried out using the experimental setup sketched in Fig. 1(f). The beam from a frequency-doubled, continuous wave $\mathrm{Nd:YVO_4}$ laser emitting at a wavelength of $\lambda = 532\,\mathrm{nm}$ is divided into two separate beams, each illuminating a high-resolution, programmable phase-only spatial light modulator (SLM). The first modulator (SLM1), in combination with the following two lenses and the Fourier mask, is employed to shape the nondiffracting induction beam. We address a specially calculated phase pattern to this SLM

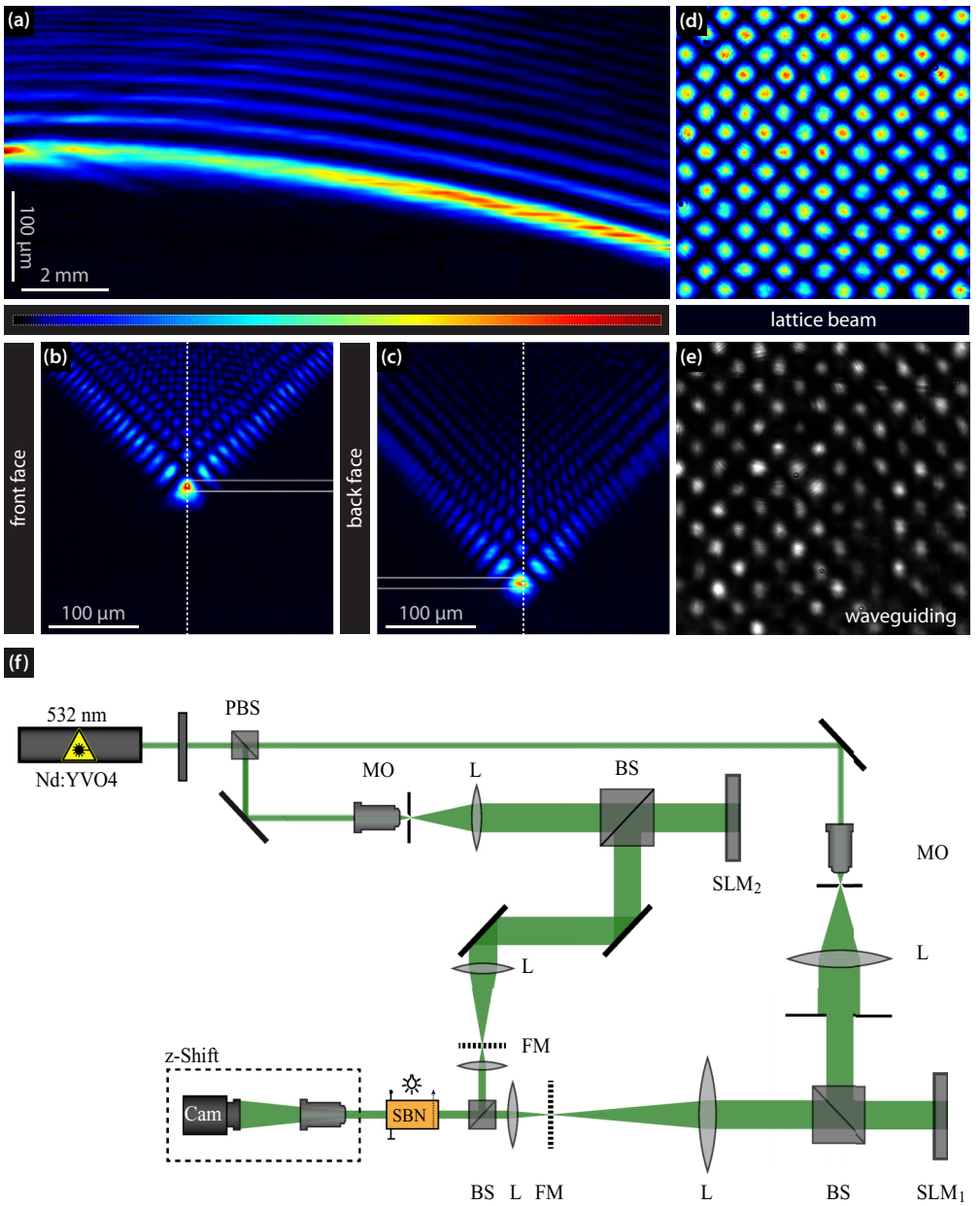

FIG. 1. (Color online) Experimental realization of two-dimensional Airy beams and photonic lattices. (a) Experimentally recorded profile during propagation, (b) intensity distribution of the Airy beam at the front face, and (c) intensity distribution at the back face. (d) Intensity pattern of the induction beam; (e) picture of the induced refractive index using wave guiding. (f) Experimental setup: (P)BS, (polarizing) beam splitter; FM, Fourier mask; L, lens; MO, microscope objective; SBN, strontium barium niobate crystal; and SLM, spatial light modulator.

which allows us to modulate the phase and the amplitude of the incident plane wave simultaneously [33]. Thereby, we obtain the complex field of the desired nondiffracting beam. Afterward, this modulated beam illuminates the 20-mm-long photorefractive $Sr_{0.60}Ba_{0.40}Nb_2O_6$ (SBN:Ce) crystal, which is externally biased with an electric dc field of $E_{ext} \approx 2000\,V/cm$ aligned along the optical c axis. To minimize the feedback of the written refractive index structure onto the induction beam itself, the induction beam is set to be ordinarily polarized with respect to the crystal's optical c axis. The high polarization anisotropy in the electro-optic coefficients of SBN:Ce [34], however, allows us to induce sufficient refractive index modulations to substantially affect the propagation of the extraordinarily polarized Airy beam. The Airy beam is realized in the same manner by directly encoding the complex field calculated in real space with Eq. (2) onto the second modulator (SLM2). To accurately overlay the two beams in the crystal, a beam splitter is placed directly in front of the SBN crystal. In addition, by illuminating the crystal homogeneously with white light, we can erase written refractive index modulations. By means of an imaging lens and a camera mounted on a translation stage we can record the intensity distribution in different transverse planes.

We support our experiments with comprehensive numerical simulations by solving the paraxial wave equation (1), which models the light propagation in media with inhomogeneous

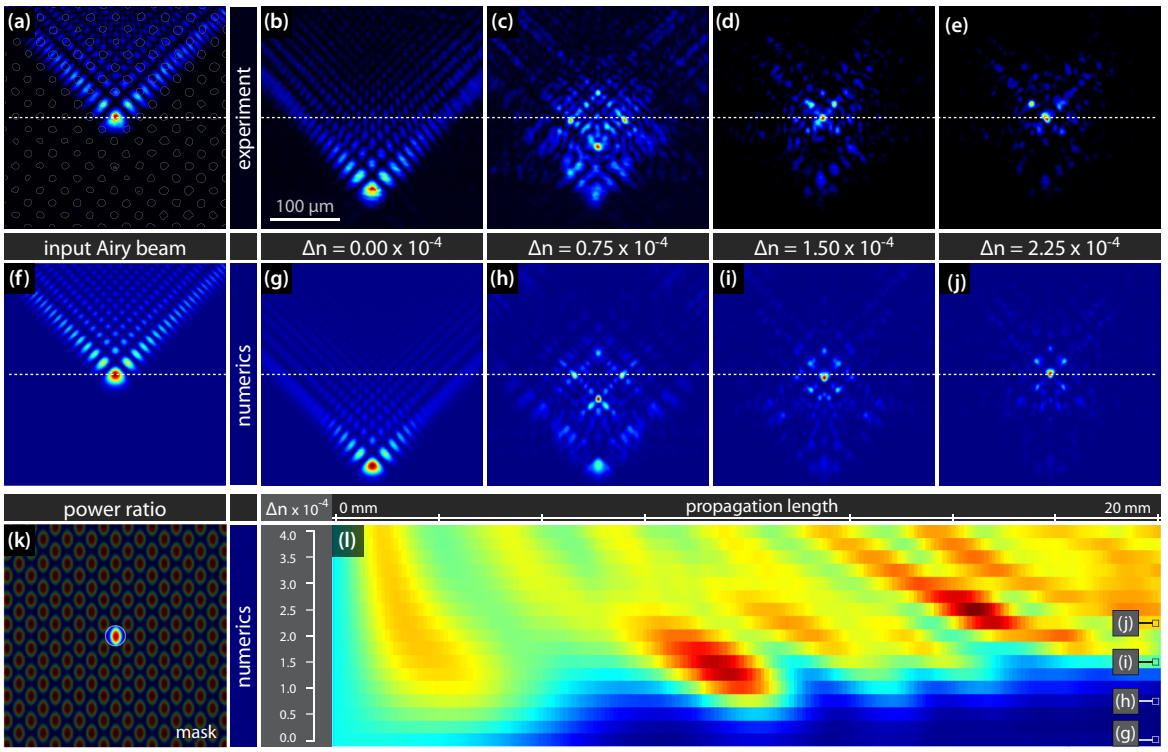

FIG. 2. (Color online) Airy beam propagation in a regular diamond lattice. (a), (f) Input Airy beams at the front crystal face in experiment and numerics [the layout of the lattice beam is indicated by open circles in panel (a)]. (b)–(e) Experimental recorded intensity distributions at the back face for different refractive index change Δn; (g)–(j) corresponding numerical results. (k) The shaded area represents the mask for the calculation of power ratio. (l) Dependance of the percentage of the Airy beam power in the incident waveguide on refractive index change Δn and propagation length z.

refractive index modulations. The resulting optically induced index modulation in the photorefractive material is represented by $\Delta n^2(I_{\mathrm{indu}})$, which can be calculated in the full anisotropic model [21] with a relaxation method. Since only linear effects are considered, the inducing intensity I_{indu} is solely given by the intensity of the nondiffracting beam, $I_{\mathrm{indu}} = |E_{\mathrm{ndB}}|^2$ [cf. Eq. (4)]. Even though the paraxial wave equation stays in the linear regime, it is not solvable analytically and we need to rely on proven beam propagation methods. The propagation equation (1) is solved numerically, using a split-step Fourier method described earlier in Ref. [35,36].

III. TWO-DIMENSIONAL AIRY BEAMS IN PHOTONIC LATTICES

In this section, we investigate the influence of an optically induced photonic lattice onto the self-acceleration of two-dimensional optical Airy beams. We set our focus on the competition between the self-bending propagation of Airy beams and the waveguiding and discrete diffraction effects of the photonic lattice. Therefore, we successively increase the strength of the induced refractive index modulation and observe the effect on the beam acceleration. While increasing the lattice strength, the Airy beam more efficiently excites different linear Bloch modes of the lattice which hinders the acceleration during propagation of the undisturbed Airy beam. This results in an effectively slowed down acceleration, which for a certain value was effectively stopped completely.

Figure 2 summarizes our results with respect to the propagation of the Airy beam inside a regular photonic lattice. The top row [Figs. 2(a)–2(e)] contains our experimental results, while the corresponding numerical simulations are shown in the second row [Figs. 2(f)–2(j)]. The first two columns recap the typical transverse displacement of the Airy beam that propagated between the front face [Figs. 2(a) and 2(f)] and the back face [Figs. 2(b) and 2(g)] of the homogenous crystal. Now, the Airy beam is launched into the induced photonic lattice with the main lobe exactly located at one lattice site. As the refractive index modulation strength growths, the interaction of the Airy beam with the lattice sites becomes stronger and consequently the bending of the Airy beam is decreased. Our experimental results [Figs. 2(c)–2(e)], as well as our numerics [Figs. 2(h)–2(j)] clearly show the frustration of the self-acceleration of the Airy beam. Depending on the different lattice strengths, various kinds of discrete structures arise until the lattice finally suppresses the acceleration of the Airy beam completely. Most of the energy then stays in the lattice site, where the main lobe of the Airy beam was initially launched.

To get a more detailed insight into the propagation dynamics, we monitor the ratio between the power guided in the central waveguide and the total power of the Airy beam as a function of the lattice strength and the propagation distance. In Fig. 2(l) the numerical results for this power ratio are shown. With this reduced representation we are able to illustrate the key signature of the complex evolution of the Airy beam during the propagation for the different lattice strengths. It illustrates,

spatially resolved, how much energy is guided in the central lattice site and thus how strong the Airy beam acceleration is frustrated by the lattice. The shaded area in Fig. 2(k) represents the mask to calculate the power in the central waveguide. This graph clearly demonstrates the impact of optically induced photonic lattice on the formation of discrete structures, as well as suppression of the acceleration and bending of the Airy beam. For certain values of Δn one can see oscillations of the beam power in the central waveguide along the propagation distance. This is due to the self-bending property of Airy beams and the influence of the central waveguide not only on the main lobe but also on other lobes that overlap with this particular waveguide along the propagation. As a result, the part of their power is monitored in the central waveguide for some propagation distances. For higher refractive index modulations Δn, one can observe the localization of most of the beam power to central waveguide as the beam leaves the crystal. Again, to experimentally control the index modulation depth we take advantage of the time-dependent buildup of the induced lattice, which grows monotonously with the writing time.

In contrast to a corresponding situation of one-dimensional Airy beams propagating in a waveguide array [18], here the localization of the two-dimensional Airy beams at the output strongly depends on the strength of the photonic lattice, which also can be seen at the right edge of Fig. 2(l). This different behavior can be explained by the fact that in two dimensions each lattice site has four next neighbors (in the one-dimensional case only two). Thus, here the interaction of the Airy beam which is launched with its main lobe exactly placed at one lattice site is more pronounced.

This dependency of the beam localization on the lattice strength, for example, can be harnessed to realize a fast switch or router for Airy beams based on their polarization. The optical induction in SBN leads to an internal space charge field that modulates the refractive index via the linear electrooptic effect. Because of the strong polarization anisotropy of the electrooptic coefficients, $r_{13} \ll r_{33}$ [34], the lattice strength experienced by the Airy beam strongly depends on the polarization. Consequently, the shape as well as center of mass of the intensity distribution that leaves the photonic lattice can be controlled solely by changing the polarization of the incoming Airy beam.

We also study the transition of the Airy beam that leaves the SBN crystal with the inscribed photonic lattice to a linear medium (e.g., air) and its further propagation. It has been shown recently that only an Airy beam initially driven by a particular self-defocusing nonlinearity experiences anomalous diffraction and can maintain its shape over a long distance after exiting the nonlinear medium [37]. In our crystal with optically induced photonic lattice we could not observe that the exiting field pattern propagates robustly with the properties characteristic for Airy beams over a long distance after the crystal.

IV. AIRY BEAM PROPAGATION IN PHOTONIC LATTICE WITH DIFFERENT DEFECTS

Besides the influence of regular photonic lattices on the behavior of two-dimensional Airy beams, we investigate the propagation effects caused by defects embedded in these lattices. In particular, we consider two-dimensional single-site defect lattices with positive or negative variable defect strengths.

To realize the different defect lattices, we use a well-localized zero-order nondiffracting Bessel beam to locally increase or decrease the refractive index modulation at one selected lattice site. It is important that the resulting defect lattice remains two-dimensional. Therefore, the lattice is induced by an effective intensity distribution resulting from an incoherent superposition of the discrete and the Bessel nondiffracting beam. This incoherent superposition is essential to get rid of the phase relation between both beams, which otherwise would lead to additional undesired intensity modulations due to interference. To avoid the coherent effects, we illuminate the crystal one after the other with the discrete and the Bessel beam, respectively. Thereby, we utilize the high dielectric response time of the SBN crystal for the used intensities that allows for switching frequencies in the order of seconds. As shown in the past, this multiplexing method is capable of fabricating a whole set of two-dimensional aperiodic structures, superlattices, and defect lattices [38–40]. In order to realize negative defects, the index modulation at one selected lattice site is decreased by switching to defocusing nonlinearity while the crystal is illuminated with the Bessel beam. This is achieved by applying the static electric field antiparallel to the optical c axis [40].

Figure 3 illustrates the basic scheme of the defect realization using multiplexed nondiffracting beams. The regular lattice is induced with the intensity distribution shown in Fig. 3(a). Simultaneously, the Bessel beam intensity shown in Fig. 3(b) increases or decreases the induced refractive index at one lattice site, depending on the direction of the applied electrical field. The resulting effective intensity distributions for the positive and negative defect lattices are shown in Figs. 3(c) and 3(d), respectively. Figures 3(e) and 3(f) show the numerically calculated refractive index modulations that result for both types of defect lattices.

Once the defect lattices are realized, we finally study how the different defects influence the Airy beam propagation and acceleration. We keep all parameters from the previous

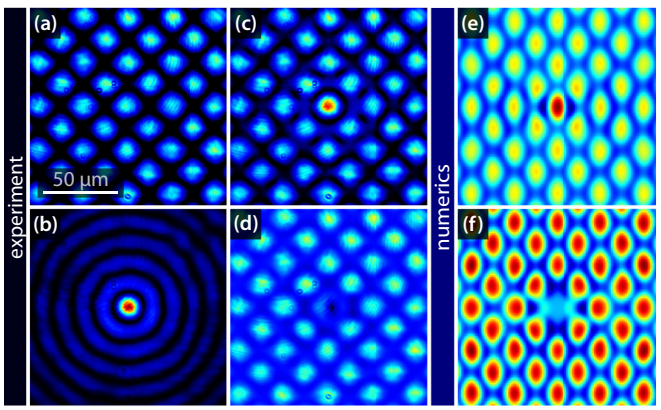

FIG. 3. (Color online) Defect generation in optically induced photonic lattice. (a) Experimental realization of the diamond lattice, (b) the Bessel beam, (c) the positive defect lattice, and (d) the negative defect lattice. Numerical realization of (e) positive and (f) negative lattice defects.

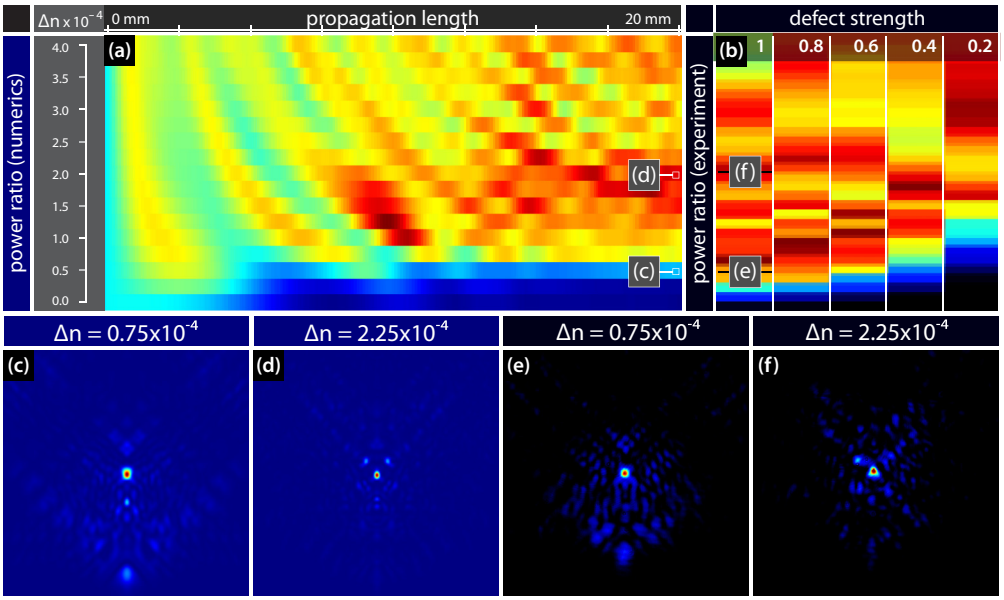

FIG. 4. (Color online) Airy beam propagation in different positive defect lattices. (a) Numerical results for the dependance of the Airy beam power propagating in defect site on refractive index change Δn and propagation length z. (b) Experimentally observed percentage of the Airy beam power propagating in the defect site as a function of the refractive index change Δn and defect strength S_{d}. (c), (d) Exemplary numerical results of Airy beam intensity distribution at the back crystal face. (e), (f) Experimentally recorded output intensity distributions. The letters in panels (a) and (b) indicate the corresponding intensity pictures.

experiments, but change the sign of the defect to both positive and negative. The Airy beam is positioned with its main lobe exactly located at the defect site. For the different defects, we record the intensity profiles of the propagated Airy beam at the back face of the crystal and monitor the percentage of the power guided in the central waveguide, as described previously.

In Figs. 4 and 5 we show our results for the positive and negative defects, respectively. The numerical results for the power ration as a function of the propagation distance ζ and the refractive index modulation Δn are presented as panels (a) in both figures. We picked two particular cases with $\Delta n = 0.75 \times 10^{-4}$ [panel (c)] and $\Delta n = 2.25 \times 10^{-4}$ [panel (d)] for representation and show the intensity profile at the back face

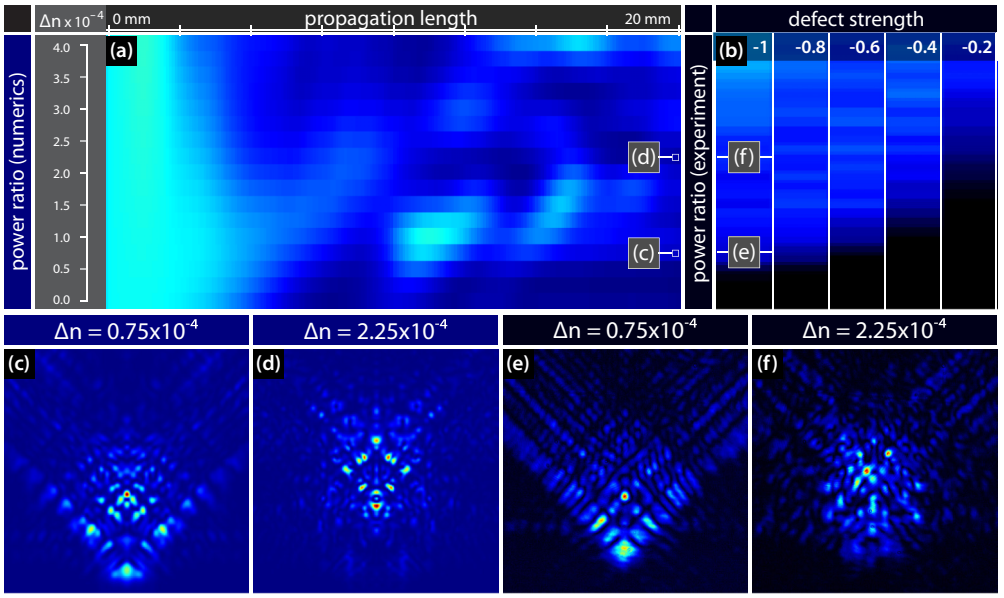

FIG. 5. (Color online) Airy beam propagation in different negative defect lattices. (a) Numerical results for the dependance of the Airy beam power propagating in defect site on refractive index change Δn and propagation length z. (b) Experimentally observed percentage of the Airy beam power propagating in the defect site as a function of the refractive index change Δn and defect strength S_{d}. (c), (d) Exemplary numerical results of Airy beam intensity distribution at the back crystal face. (e), (f) Experimentally recorded output intensity distributions. The letters in panels (a) and (b) indicate the corresponding intensity pictures.

of the crystal. The positions corresponding to these intensity profiles are indicated with the letters (c) and (d) in the power ratio plot (a).

Because in experiments it is not possible to record the intensity pattern inside an inhomogeneous crystal, we are restricted to the profiles at the back face. In Figs. 4(b) and 5(b) the experimentally measured power ratio at the back face is plotted as a function of the refractive index modulation and the defect strength. Therefore, we have repeated the experiments for five different defect strengths for both positive and negative defects and recorded the intensity profile at the back face. The modulus of the defect strength S_d is given by the ratio of the peak intensities of the discrete and the Bessel nondiffracting beam, while the sign is determined by the direction of the applied electric field. In the experiment, we also select the two representative lattice strengths Δn to show the intensity profile at the output of the crystal [panels (e) and (f)]. Again, their positions in the experimental power ratio plot (b) are indicated with the letters (e) and (f).

These results illustrate the strong dependence of the propagation and acceleration properties of the Airy beam on the lattice depths, as well as the defect strength. The positive defect [Fig. 4(a)] strongly enhances the localization of the Airy beam, while for the negative defect [Fig. 5(a)] the power guided in the defect site is significantly reduced and finally completely repelled. A similar behavior was reported earlier for one-dimensional Airy beams propagating in a waveguide array with defects [18], and it was predicted that it qualitatively agrees with the results in two dimensions.

V. CONCLUSION

In summary, we have demonstrated the control over the propagation dynamics of two-dimensional Airy beams in optically induced photonic lattices. We have shown, both theoretically and experimentally, that depending on the depths of the induced lattice, the acceleration and the bending of the Airy beam are strongly affected. For increasing refractive index contrast, different discrete patterns arise and for a certain value the acceleration of the beam is effectively stopped. Moreover, we demonstrated the influence of various single-side defects on the propagation dynamics of the Airy beam. The defect strength as well as the lattice depth dramatically change the initial Airy beam shape and its self-bending. For positive defects, the localization is remarkably increased, while for negative defects, the situation is changed to transport nearly no power along the defect site. All presented experimental results fully agree with the supporting numerical simulations. Our results can readily be generalized to other kinds of optically induced lattices and defect types, including more complex or even three-dimensional lattices. Also other classes of self-accelerated optical beams can be controlled using the presented ideas and methods.

ACKNOWLEDGMENTS

This work is partially supported by the German Academic Exchange Service (Project 56267010) and Ministry of Education, Science and Technological Development, Republic of Serbia (Project OI 171036).

[1] M. V. Berry and N. L. Balazs, Am. J. Phys. **47**, 264 (1979).
[2] G. A. Siviloglou, J. Broky, A. Dogariu, and D. N. Christodoulides, Phys. Rev. Lett. **99**, 213901 (2007).
[3] T. Ellenbogen, N. Voloch-Bloch, A. Ganany-Padowicz, and A. Arie, Nat. Photonics **3**, 395 (2009).
[4] D. Abdollahpour, S. Suntsov, D. G. Papazoglou, and S. Tzortzakis, Phys. Rev. Lett. **105**, 253901 (2010).
[5] A. Chong, W. H. Renninger, D. N. Christodoulides, and F. W. Wise, Nat. Photon. **4**, 103 (2010).
[6] G. A. Siviloglou, J. Broky, A. Dogariu, and D. N. Christodoulides, Opt. Lett. **33**, 207 (2008).
[7] Y. Hu, P. Zhang, C. Lou, S. Huang, J. Xu, and Z. Chen, Opt. Lett. **35**, 2260 (2010).
[8] W. Liu, D. N. Neshev, I. V. Shadrivov, A. E. Miroshnichenko, and Y. S. Kivshar, Opt. Lett. **36**, 1164 (2011).
[9] N. K. Efremidis and D. N. Christodoulides, Opt. Lett. **35**, 4045 (2010).
[10] J. Baumgartl, M. Mazilu, and K. Dholakia, Nat. Photon. **2**, 675 (2008).
[11] P. Rose, F. Diebel, M. Boguslawski, and C. Denz, Appl. Phys. Lett. **102**, 101101 (2013).
[12] N. K. Efremidis, Opt. Lett. **36**, 3006 (2011).
[13] Z. Ye, S. Liu, C. Lou, P. Zhang, Y. Hu, D. Song, J. Zhao, and Z. Chen, Opt. Lett. **36**, 3230 (2011).
[14] S. Chávez-Cerda, U. Ruiz, V. Arrizón, and H. M. Moya-Cessa, Opt. Express **19**, 16448 (2011).
[15] N. K. Efremidis and I. D. Chremmos, Opt. Lett. **37**, 1277 (2012).
[16] I. D. Chremmos and N. K. Efremidis, Phys. Rev. A **85**, 063830 (2012).
[17] I. D. Chremmos and N. K. Efremidis, J. Opt. Soc. Am. A **29**, 861 (2012).
[18] N. M. Lučić, B. M. Bokić, D. Ž. Grujić, D. V. Pantelić, B. M. Jelenković, A. Piper, D. M. Jović, and D. V. Timotijević, Phys. Rev. A **88**, 63815 (2013).
[19] A. Piper, D. V. Timotijević, and D. M. Jović, Phys. Scr. **T157**, 014023 (2013).
[20] N. K. Efremidis, S. Sears, D. N. Christodoulides, J. W. Fleischer, and M. Segev, Phys. Rev. E **66**, 046602 (2002).
[21] A. A. Zozulya and D. Z. Anderson, Phys. Rev. A **51**, 1520 (1995).
[22] I. M. Besieris and A. M. Shaarawi, Opt. Lett. **32**, 2447 (2007).
[23] G. A. Siviloglou and D. N. Christodoulides, Opt. Lett. **32**, 979 (2007).
[24] B. Terhalle, D. Träger, L. Tang, J. Imbrock, and C. Denz, Phys. Rev. E **74**, 057601 (2006).
[25] P. Rose, M. Boguslawski, and C. Denz, New J. Phys. **14**, 033018 (2012).
[26] J. Xavier, P. Rose, B. Terhalle, J. Joseph, and C. Denz, Opt. Lett. **34**, 2625 (2009).
[27] T. Schwartz, G. Bartal, S. Fishman, and M. Segev, Nature (London) **446**, 52 (2007).
[28] J. W. Fleischer, M. Segev, N. K. Efremidis, and D. N. Christodoulides, Nature (London) **422**, 147 (2003).

[29] B. Terhalle, T. Richter, A. S. Desyatnikov, D. N. Neshev, W. Krolikowski, F. Kaiser, C. Denz, and Y. S. Kivshar, Phys. Rev. Lett. **101**, 013903 (2008).
[30] N. V. Kukhtarev, V. B. Markov, S. G. Odulov, M. S. Soskin, and V. L. Vinetskii, Ferroelectrics **22**, 949 (1978).
[31] J. Durnin, J. J. Miceli, and J. H. Eberly, Phys. Rev. Lett. **58**, 1499 (1987).
[32] Z. Bouchal, Czechoslov. J. Phys. **53**, 537 (2003).
[33] J. A. Davis, D. M. Cottrell, J. Campos, M. J. Yzuel, and I. Moreno, Appl. Opt. **38**, 5004 (1999).
[34] U. B. Dörfler, R. Piechatzek, T. Woike, M. K. Imlau, V. Wirth, L. Bohatý, T. Volk, R. Pankrath, and M. Wöhlecke, Appl. Phys. B: Lasers Opt. **68**, 843 (1999).
[35] M. R. Belić, J. Leonardy, D. V. Timotijević, and F. Kaiser, J. Opt. Soc. Am. B **12**, 1602 (1995).
[36] M. R. Belić, M. S. Petrović, D. M. Jović, A. Strinić, D. Arsenović, K. Motzek, F. Kaiser, P. Jander, C. Denz, M. Tlidi, and P. Mandel, Opt. Express **12**, 708 (2004).
[37] Y. Hu, S. Huang, P. Zhang, C. Lou, J. Xu, and Z. Chen, Opt. Lett. **35**, 3952 (2010).
[38] F. Diebel, D. Leykam, M. Boguslawski, P. Rose, C. Denz, and A. Desyatnikov, Appl. Phys. Lett. **104**, 261111 (2014).
[39] M. Boguslawski, A. Kelberer, P. Rose, and C. Denz, Opt. Express **20**, 27331 (2012).
[40] M. Boguslawski, A. Kelberer, P. Rose, and C. Denz, Opt. Lett. **37**, 797 (2012).